J. Electrochem. Sci. Eng. **16** (2026) 3085; https://doi.org/10.5599/jese.3085

Open Access : : ISSN 1847-9286
https://pub.iapchem.org/ojs/index.php/JESE

Original scientific paper

Ferrocenium tetrachloromagnesate modified MWCNTs electrode for detection of Bi^{3+} at the trace level in polluted aqueous solutions

Rahadian Zainul[1], Alwi Nofriandi[2], Norhayati Hashim[3], Mohamad Idris Saidin[3], Mohamad Syahrizal Ahmad[3], Siti Nur Akmar Mohd Yazid[3], Sharifah Norain Mohd Sharif[3], Wan Rusmawati Wan Mahamod[3] and Illyas Md Isa[3,✉]

[1]*Department of Chemistry, Faculty of Natural Science and Mathematics, Universitas Negeri Padang, 25132 Air Tawar, Padang, Indonesia*
[2]*Doctoral Program of Environmental Science, Postgraduate Program, Universitas Negeri Padang, 25132 Air Tawar, Padang Indonesia*
[3]*Department of Chemistry, Faculty of Science and Mathematics, Universiti Pendidikan Sultan Idris, 35900 Tanjong Malim, Perak, Malaysia*

Corresponding Author: ✉illyas@fsmt.upsi.edu.my

Received: October 22, 2025; Accepted: December 30, 2025; Published: January 5, 2026

Abstract

This study presents the fabrication of a ferrocenium tetrachloromagnesate (FTM) modified multi-walled carbon nanotubes (MWCNTs) electrode for the voltammetric determination of bismuth ions (Bi^{3+}) in aquatic environments. The FTM was synthesized from the reaction of magnesium chloride with ferrocene. The incorporation of FTM, a redox-active species, was shown to markedly improve electron transfer kinetics and overall electrochemical conductivity. Structural and morphological characterizations via Fourier transform infrared spectroscopy, transmission electron microscopy, energy dispersive x-ray, field emission scanning electron microscopy and X-ray diffraction confirmed the successful embedding of FTM within the electrode matrix. Electrochemical assessments using cyclic voltammetry, electrochemical impedance spectroscopy, and chronocoulometry revealed that a 10 wt.% FTM loading provided the most optimal charge transfer and interfacial behaviour. Differential pulse stripping voltammetry further demonstrated the high sensitivity of the developed electrode, achieving an ultralow detection limit of 0.543 nM with two broad linear ranges of 1.0 nM to 0.1 and 1.0 µM to 0.1 mM for Bi^{3+}. The sensor also exhibited remarkable reproducibility (RSD 8.67 %) and stability (RSD 7.77 %). Furthermore, excellent selectivity toward Bi^{3+} was maintained in the presence of potentially interfering ions such as Mn^{2+}, La^{3+}, Ni^{2+}, Li^{+}, Zn^{2+}, Fe^{2+}, Cd^{2+}, Cu^{2+}, Er^{2+} and Pb^{2+}. Real water-sample analyses yielded recoveries of 89 to 104 %, confirming the practical feasibility of the electrode for environmental monitoring.

Keywords
Magnesium containing complex; organometallic compound; electroactive modifier, heavy metal detection; environmental (water) samples

Introduction

Bismuth (Bi) is a heavy metal widely used in catalysis [1], cosmetics [2] and pharmaceuticals [3], but its presence in aquatic environments at elevated levels raises ecological and health concerns [4-6]. The accumulation of Bi^{3+} in water can disturb aquatic ecosystems and compromise water quality, necessitating reliable monitoring strategies [7]. Conventional laboratory-based methods, such as inductively coupled plasma-mass spectrometry (ICP-MS) and atomic absorption spectroscopy (AAS) provide highly accurate detection of trace metals [8,9]; however, their high operational costs, complex sample preparation procedures, and limited portability restrict their use for routine and in situ environmental monitoring.

Electrochemical sensing has emerged as a practical alternative, offering rapid response, portability, and cost-effectiveness, making it suitable for real-time environmental monitoring [10,11]. Among electrochemical platforms, carbon paste electrodes (CPEs) have gained considerable attention due to their low background current, ease of surface renewal, chemical inertness, and versatility in incorporating various modifiers. Recent reviews have emphasized the growing use of CPE-based composite electrodes, including MWCNTs-modified carbon pastes, in enhancing electron transfer kinetics, improving sensitivity, and enabling selective detection of heavy metals in aqueous matrices [12,13]. Such developments highlight the importance of material engineering in optimizing electrode performance.

The performance of electrochemical sensors largely depends on the design of electrode materials and their ability to mediate electron transfer while maintaining selectivity for the analyte of interest [14-16]. Consequently, electroactive modifiers that combine strong redox activity, stability, and structural tunability have attracted increasing attention in recent years [17,18]. Among these, ferrocene (Fc), an organometallic compound with a reversible Fe^{2+}/Fe^{3+} redox couple, has been extensively employed in sensing applications due to its stable electrochemical behaviour and capacity for electron mediation [19].

The role of alkaline earth metals, particularly magnesium, in the development of ferrocene-based sensing systems has received comparatively little attention. Magnesium is an abundant, lightweight, and biocompatible metal, which distinguishes it from many other metallic components used in functional materials [20,21]. While magnesium alloys have been extensively investigated in structural and biomedical contexts, the functional chemistry of magnesium in hybrid complexes remains underexplored, particularly in electroanalytical applications [22]. Magnesium offers distinct advantages: as a divalent cation, Mg^{2+} provides strong ionic stabilization without introducing toxicity concerns, and when incorporated into chlorometallate frameworks, it can improve structural robustness and influence the electronic environment of adjacent redox-active centres [23]. These features suggest that magnesium-based complexes could play a unique role in enhancing charge transport and interfacial stability in electrochemical sensors.

In the broader field of magnesium alloys, research has primarily focused on improving corrosion resistance [24], catalytic activity [25], and biomedical performance [26]. However, translating magnesium chemistry into the realm of sensing technologies opens new avenues for multifunctional applications. In this study, ferrocenium tetrachloromagnesate (FTM) is introduced as a novel magnesium-based complex specifically designed for the electrochemical detection of Bi^{3+} ions. The

compound integrates the reversible redox behaviour of ferrocenium (Fc^+) with the stabilizing role of Mg^{2+} in a chlorometallate framework. This dual functionality is expected to combine robust electron transfer kinetics with enhanced structural and interfacial stability, thereby enabling selective and sensitive detection of Bi^{3+} ions in aqueous environments.

Previous studies have highlighted the versatile role of magnesium in a wide range of scientific disciplines. In catalysis, magnesium has been explored as an effective material for hydrogen production through thermochemical water splitting, although its application is limited by slow Mg-water reaction kinetics [27]. In biomedical research, magnesium is valued for its biocompatibility and mechanical properties similar to those of bone, making it attractive for biodegradable implants; however, its rapid corrosion remains a major challenge [28]. Furthermore, magnesium oxide (MgO) has shown excellent adsorption performance for hazardous ions such as arsenate, highlighting its potential for environmental remediation [29]. Collectively, these findings underscore magnesium's potential as a stable and functional material, although its integration into electrochemical systems, particularly for sensing applications, remains relatively underexplored.

This study highlights the broader potential of magnesium compounds in a functional material design. By demonstrating the capability of a magnesium-based complex in environmental monitoring, the application scope of magnesium is extended beyond its established roles in structural alloys, biomedical devices, and catalysis. The findings provide new insights into the structure-function relationship of magnesium-containing complexes and establish FTM as both a cost-effective sensing material and a representative example of how magnesium chemistry can be harnessed in advanced electroanalytical technologies. In doing so, the present work bridges electrochemistry with magnesium materials science and aligns with the growing trend toward diversifying magnesium alloys and compounds for multifunctional technological applications.

Experimental

Apparatus and chemicals

In this work, pH values were determined using an Orion 72A+ pH meter (USA) equipped with a glass electrode. Electrochemical experiments, including cyclic voltammetry (CV), differential pulse stripping voltammetry (DPSV), and chronocoulometry, were carried out with a Gamry Series-G750 potentiostat (USA). A conventional three-electrode configuration was employed, consisting of an Ag/AgCl (3.0 M KCl) reference electrode (MF-2052, Bioanalytical Systems, USA), a platinum wire as the counter electrode, and an MWCNT-based carbon paste electrode as the working electrode. The components were manually homogenized, and the resulting paste was packed into a Teflon holder with a copper wire for electrical contact; the electrode surface was gently polished prior to use. Electrochemical impedance spectroscopy (EIS) measurements were performed using a Gamry Potentiostat/Galvanostat Ref 3000 (USA). The supporting electrolytes tested included NaCl, KCl, KNO_3, Na_2SO_4 and $NaNO_3$. Bismuth (Bi^{3+}) was selected as the target analyte, with pH adjustment achieved using 0.1 M NaOH and 0.1 M HCl solutions. To assess potential interferences, cations such as Mn^{2+}, La^{3+}, Ni^{2+}, Li^+, Zn^{2+}, Fe^{2+}, Cd^{2+}, Cu^{2+}, Er^{2+}, Ca^{2+}, and Pb^{2+} (all purchased from Sigma-Aldrich, USA) were evaluated. All solutions were freshly prepared with deionized water.

Synthesis of ferrocenium tetrachloromagnesate

The synthesis of FTM was conducted using magnesium(II) chloride dissolved and ferrocene dissolved in ethanol, each prepared in a separate 10 mL beaker. To ensure thorough mixing, the magnesium(II) chloride solution was added dropwise to the ferrocene solution under continuous

stirring, during which the colour gradually changed to a deep green. The mixture was stirred for 1 h and then left undisturbed for 7 days to allow further reaction and precipitation. Afterward, the solution was carefully transferred into a measuring cylinder and kept for an additional 24 h. The resulting precipitate was then separated by filtration, yielding a black-coloured material, which was subsequently collected and used as a modifier for electrode preparation.

Fabrication of electrode

To construct the electrodes, a fixed amount of MWCNTs (100 mg, >95 % carbon basis, outer diameter 10 to 20 nm, length 10 to 30 µm; Sigma-Aldrich) was combined with FTM at different loadings (0.0, 5.0, 10.0 and 15.0 wt.%). These mixtures, corresponding to overall compositions of 100.0, 95.0, 90.0 and 85.0 wt.%, were ground in a mortar until homogeneity is attained. Three drops of paraffin oil (high-purity mineral oil, viscosity ~65 $mm^2\ s^{-1}$ at 40 °C; Merck) were then added as a binder, and the blends were further mixed to form a uniform paste. The obtained material was subsequently packed into Teflon tubes (2.0 mm inner diameter, 3.0 cm length). For electrical contact, mercury was used to seal one end of the tube, and a copper wire served as the external lead. Prior to electrochemical measurements, the electrode surface was renewed by gentle polishing with filter paper. Control electrodes were prepared identically, but without FTM.

Electrochemical detection of Bi^{3+}

Electrochemical analyses of Bi^{3+} were carried out using an FTM-modified electrode in 0.05 M KCl-HCl supporting electrolyte at pH 0.5. Differential pulse stripping voltammetry (DPSV) was applied under the following parameters: pulse amplitude of 25 mV, step potential of 5 mV, pulse increment of 2.5 mV, pulse duration of 0.1 s, accumulation period of 150 s, and equilibration time of 25 s. The potential window was scanned from -0.65 to -0.3 V, with the oxidation peak observed at -0.47 V. All measurements were performed at room temperature (25 ± 2 °C).

Sample preparation and conditioning procedures

In this study, water samples were collected from four inactive mining rivers in the Keliang and Kalumpang regions of Malaysia. Immediately after collection, the samples were sealed in sterile containers and preserved at 4 °C to suppress microbial growth and restrict chemical alterations. For electrochemical analysis, 25.00 mL portions of the stored water were measured into volumetric flasks pre-filled with 0.05 M KCl, which served as the supporting electrolyte. The acidity of each solution was then adjusted to pH 0.5 using 0.1 M HCl. The samples were analysed without any external enrichment, thereby enabling direct assessment of Bi^{3+} species naturally present in the river water.

Results and discussion

Active material characterization

The active material was characterized using FTIR, TEM, EDX, FESEM and XRD techniques to confirm the successful synthesis of the FTM. FTIR identifies functional groups, TEM provides detailed visualization of the internal structure and nanoscale dispersion of materials within the composite, EDX verifies elemental composition, and FESEM observes surface morphology. Meanwhile, XRD determines the crystalline phase, structural purity, and confirms the successful formation of the target compound through the identification of characteristic diffraction peaks.

The FTIR spectrum of FTM (Figure 1a) displays several characteristic absorption bands that confirm the successful formation of the complex.

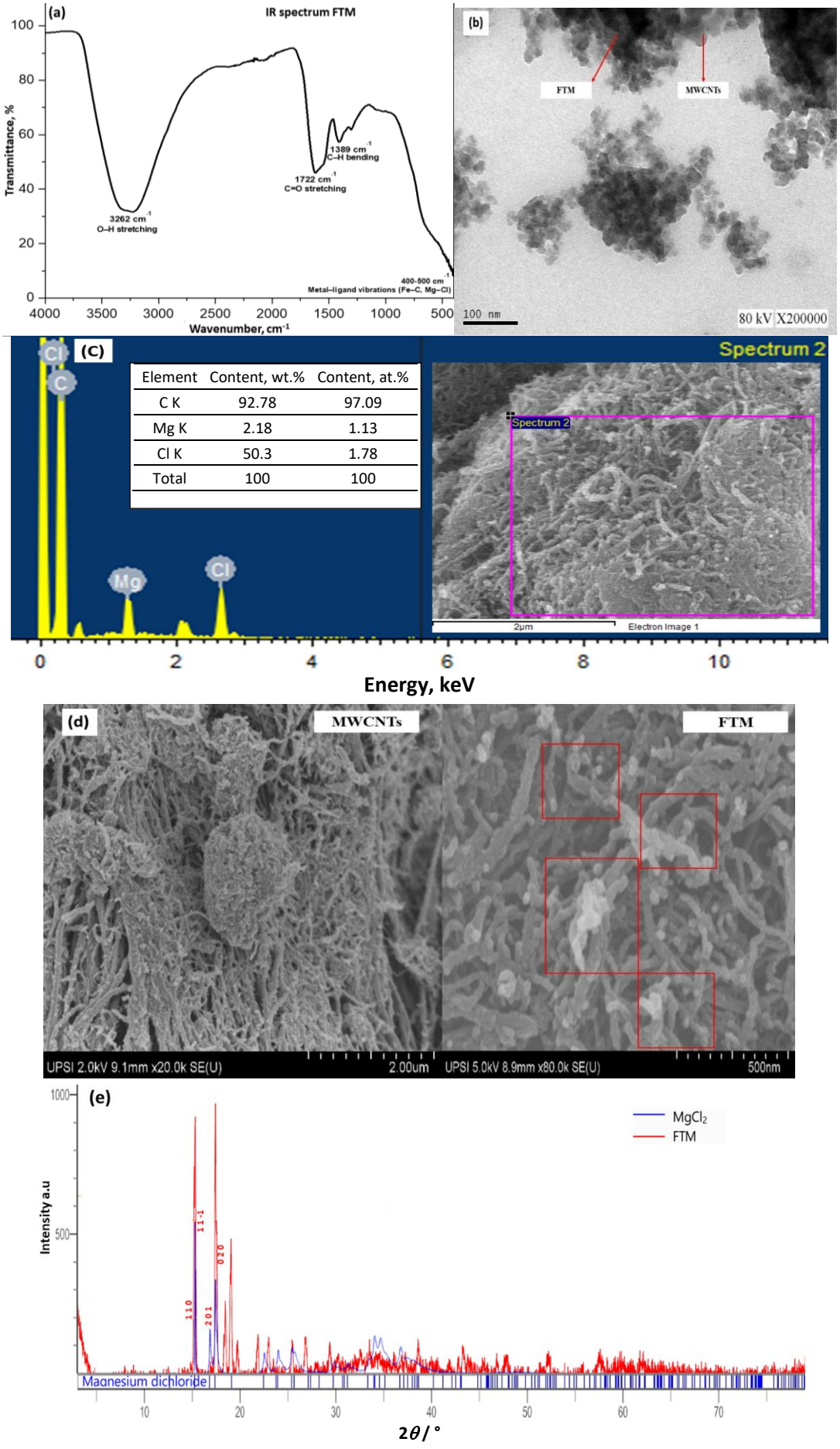

Figure 1. *(a) FTIR spectrum of FTM; (b) TEM image of MWCNTs/FTM; (c) EDX results on MWCNTs/FTM; (d) FESEM results on MWCNTs/FTM and (e) XRD patterns of FTM*

The broad band at 3262 cm^{-1} is attributed to O-H stretching vibrations, likely originating from hydroxyl groups or adsorbed water molecules, indicating the presence of hydrogen bonding interactions. The strong band observed at 1722 cm^{-1} corresponds to C=O stretching vibrations, suggesting the involvement of carbonyl groups in coordination with Mg(II) ions, thereby enhancing the stability of the complex. The absorption at 1389 cm^{-1} is assigned to the C-H bending vibrations of the cyclopentadienyl (Cp) ring, confirming that the ferrocene structure remains intact after complexation. In the lower wavenumber region (400 to 500 cm^{-1}), distinct bands associated with Fe-C and Mg-Cl vibrations are observed, providing direct evidence of metal-ligand interactions within the FTM.

The TEM image of the MWCNTs/FTM composite (Figure 1b) at 200,000× magnification reveals a networked morphology of the MWCNTs, while the FTM particles appear to be attached to the outer walls of the nanotubes and partially dispersed around them. The relatively uniform distribution of FTM particles indicates good interaction with the carbon framework, although the FTM is not fully embedded within the tubular structure, but is predominantly bound to the surface. The EDX spectrum in Figure 1c reveals that the electrode material is predominantly carbon (97.09 at.%), originating from the MWCNT matrix, while magnesium (1.13 at.%) and chlorine (1.78 at.%) signals confirm the presence of FTM on the nanotube surface. The dominance of carbon highlights the structural integrity of the MWCNT framework, whereas the detection of Mg and Cl, albeit in relatively small amounts, confirms successful modification of the electrode with the magnesium-based complex. As shown in Figure 1d, the pristine MWCNT structure appears as an open, interconnected fibrous network that forms a porous matrix with a high surface area (top panel). After modification with FTM, the surface of the MWCNTs changes with the appearance of nodular aggregates in the sub-micron to micron size range (bottom panel). These FTM aggregates are attached to the nanotube bundles and at junction points, resulting in a rougher, more heterogeneous morphology than the original nanotube network. The relatively uniform distribution of the aggregates indicates that FTM was successfully anchored onto the MWCNTs surface, providing a granular texture characteristic of the modified electrode.

The X-ray diffraction pattern (Figure 1e) exhibits several intense peaks in the 2θ range of approximately 10 to 22°, which can be indexed to the (110), (111), (201), and (020) planes corresponding to the characteristic reflections of $MgCl_2$. The presence of these dominant peaks clearly confirms the existence of crystalline $MgCl_2$ within the FTM material synthesized from ferrocene and magnesium chloride. The absence of additional diffraction peaks indicates that no significant impurity phases were formed during the synthesis, suggesting that ferrocene interacted or complexed with $MgCl_2$ without altering its fundamental crystal structure. This finding demonstrates that $MgCl_2$ remains structurally stable within the FTM framework, serving as an inorganic matrix that potentially enhances the electrochemical activity of the ferrocene-derived component.

Electrochemical properties

To evaluate the electrochemical properties of the fabricated electrodes, a series of fundamental studies, including CV, EIS, and chronocoulometry, was conducted. These complementary techniques provide comprehensive insights into the redox behaviour, interfacial charge transfer, and effective electroactive surface area of the FTM-modified electrode. CV was first employed to investigate the effect of modifier loading on redox activity, whereas EIS was used to assess the electron-transfer resistance at the electrode-electrolyte interface. Chronocoulometry further quantified the electroactive surface area.

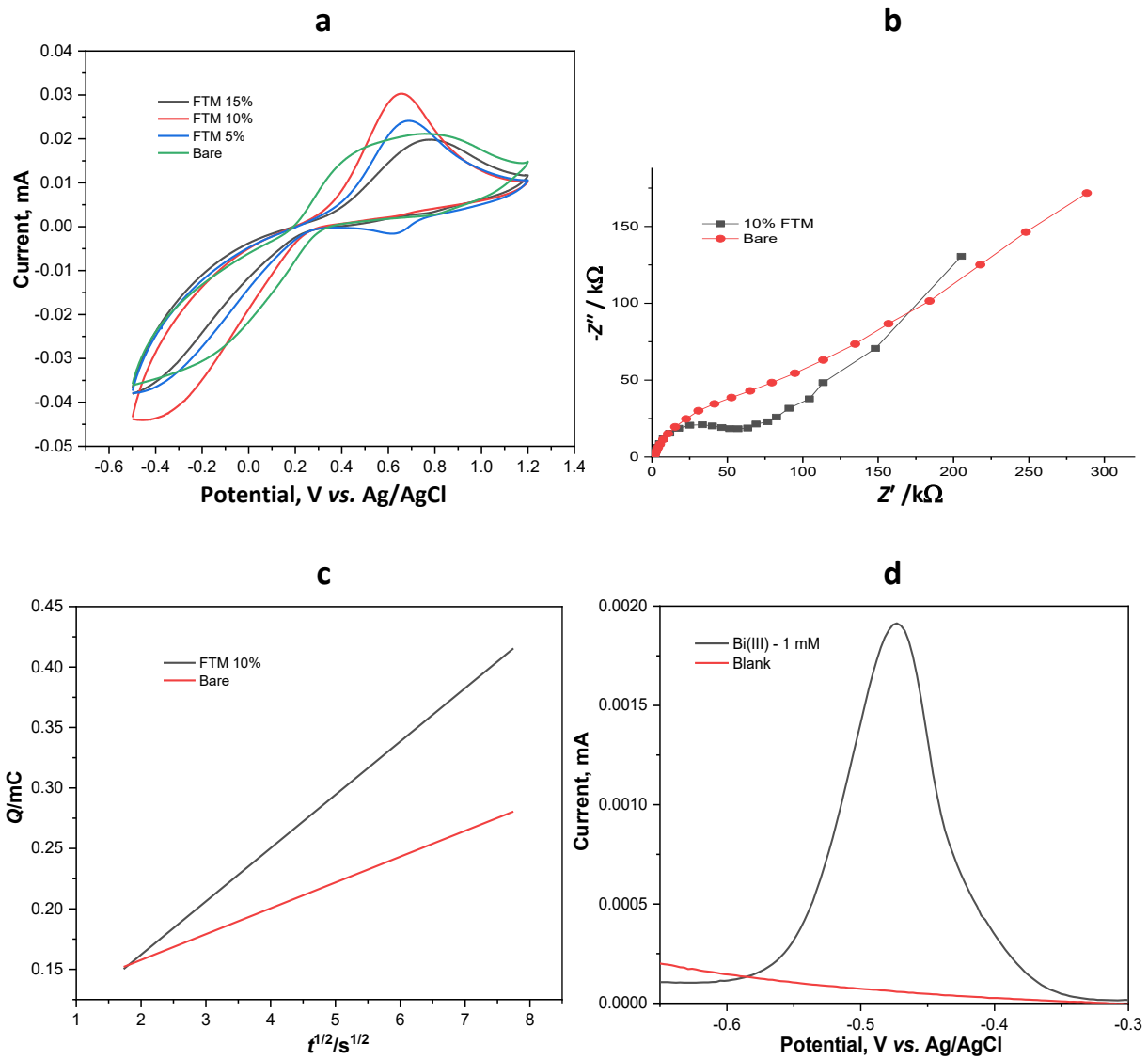

***Figure 2**. (a) CVs of bare and FTM-modified electrodes for different modifier ratio variation, at a scan rate of 100 mV s^{-1} and (b) EIS and (c) chronocoulometry data of bare and 10 wt.% FTM modified electrode in 0.05 M KCl with 10 mM $K_3[Fe(CN)_6]$; (d) differential pulse stripping voltammograms of 1 mM Bi^{3+} recorded at the bare electrode and 10 wt.% FTM-modified electrode (1.0 mM HCl in 0.05 M KCl)*

Figure 2a compares the CV responses of the bare electrode and FTM-modified electrodes with different modifier ratios (5, 10 and 15 wt.%), highlighting the superior electrochemical performance of the 10 wt.% FTM-modified electrode. The bare electrode exhibited relatively small and broad redox peaks (I_{pa} ≈ +21.1 µA; I_{pc} ≈ -34.1 µA), indicating sluggish electron transfer and limited electro-active surface area. In contrast, the 10 wt.% FTM-modified electrode showed a pronounced enhancement in both anodic and cathodic currents (I_{pa} ≈ +35.3 µA; I_{pc} ≈ -44.3 µA), with sharper and more symmetrical peaks. This improvement confirms that the incorporation of 10 wt.% FTM significantly accelerates charge transfer and increases the number of accessible electroactive sites, thereby yielding an optimal composition that enhances electrochemical performance relative to the unmodified electrode.

Quantitatively, modification with 10 wt.% FTM produces a substantial improvement in the voltammetric response compared to the bare electrode. The anodic peak current (I_{pa}) increases from 21.1 to 35.3 µA (≈67 % increase), whereas the cathodic peak current ($|I_{pc}|$) rises from 34.1 to 44.3 µA (≈30 % increase). The larger relative increase in I_{pa} indicates that the modifier preferentially enhances the oxidation process, although both the anodic and cathodic currents increase. The ratio

$I_{pa}/|I_{pc}|$ increases from ≈0.619 (bare) to ≈0.797 (10 wt.% FTM), indicating that the CV peaks become more symmetric after modification a sign of improved charge-transfer kinetics and more balanced interfacial behaviour. As shown in Figure 2b, EIS indicates that the charge-transfer resistance (R_{ct}) decreased from 112 kΩ for the bare electrode to 70 kΩ after modification with 10 wt.% FTM. The apparent heterogeneous electron-transfer rate constant (K_{app}) was calculated using Equation (1), where R is the gas constant (8.314 J mol^{-1} K^{-1}), T is the temperature (298 K), n is the number of electrons transferred (1), F is the Faraday constant (96,485 C mol^{-1}), C_A is the concentration of the redox probe (10 mM), and R_{ct} values are extracted from the Nyquist plots in Figure 1b.

$$K_{app} = \frac{RT}{F^2 R_{ct} C_A} \quad (1)$$

Using these parameters, K_{app} was determined to be 3.36×10^{-5} cm s^{-1} for the bare electrode and 5.38×10^{-5} cm s^{-1} for the 10 wt.% FTM-modified electrode, reflecting an improvement of ~60 % in electron-transfer kinetics. This result confirms that the incorporation of FTM facilitates faster interfacial charge transfer, thereby enhancing the electrochemical performance of the electrode.

Chronocoulometric analysis is used to measure the amount of electric charge generated during the redox process of an analyte and can also be used in determining the concentration of a substance in analytical chemistry. In this work, chronocoulometry was employed to evaluate the effective electrochemical surface area of both bare and FTM-modified paste electrodes. The measurements were carried out using a 10 wt.% FTM modifier in a solution containing 10 mM $K_3[Fe(CN)_6]$ and 0.05 M KCl. The effective surface area was calculated according to Anson's Equation (2) [30,31], used to determine the effective electrochemical surface area from the slope (a) of the $Q(t)$ graph plotted in Figure 2c.

$$A = \frac{a}{\left(\frac{2nFCD^{1/2}}{\pi^{1/2}}\right)} \quad (2)$$

Here, A / cm^2 represents the electroactive surface area, C / mol cm^{-3} is the concentration of the redox probe, D = 7.6×10^{-6} cm^2 s^{-1} is the diffusion coefficient of $K_3[Fe(CN)_6]$, n is the number of electrons involved, and F is the Faraday constant. In the analysis, the FTM-modified electrode exhibited an electroactive area of 1.47 mm^2, approximately twice that of the unmodified electrode (0.713 mm^2). This increase in surface area provides a higher density of active sites, thereby facilitating electrochemical reactions.

The differential pulse stripping voltammetry (DPSV) response (Figure 2d) of the FTM-modified electrode in 1.0 mM Bi^{3+} with 0.05 M KCl as supporting electrolyte shows a distinct and sharp stripping peak at around -0.47 V *vs*. Ag/AgCl with a peak current of approximately 1.9 µA, which originates from the oxidation of Bi deposits formed during the preconcentration step, confirming efficient electrochemical accumulation and subsequent stripping of Bi^{3+}. The well-defined and symmetric peak shape suggests fast electron-transfer kinetics and homogeneous deposition of bismuth facilitated by the conductive MWCNT framework and redox-active FTM sites, which together enhance charge transport and increase the electroactive surface area. In contrast, the blank signal exhibits negligible current, verifying that the response is specific to Bi^{3+} ions and not from the supporting electrolyte or the electrode matrix, thereby demonstrating the high sensitivity and selectivity of the modified electrode system.

Detection mechanism of bismuth(III) ions

The schematic illustration (Figure 3) outlines the electrochemical detection pathway of Bi^{3+} using an electrode modified with FTM. This modifier integrates the redox-active ferrocenium cation with the coordinating tetrachloromagnesate complex, forming an electroactive interface capable of enhancing the interaction between the electrode and Bi^{3+} species. The diagram highlights the sequential processes that govern stripping voltammetry, namely the accumulation of Bi^{3+}, its electrochemical reduction to metallic bismuth, and its subsequent anodic stripping during DPSV measurement. Together, these steps illustrate how FTM contributes to improving the sensitivity and reliability of Bi^{3+} detection.

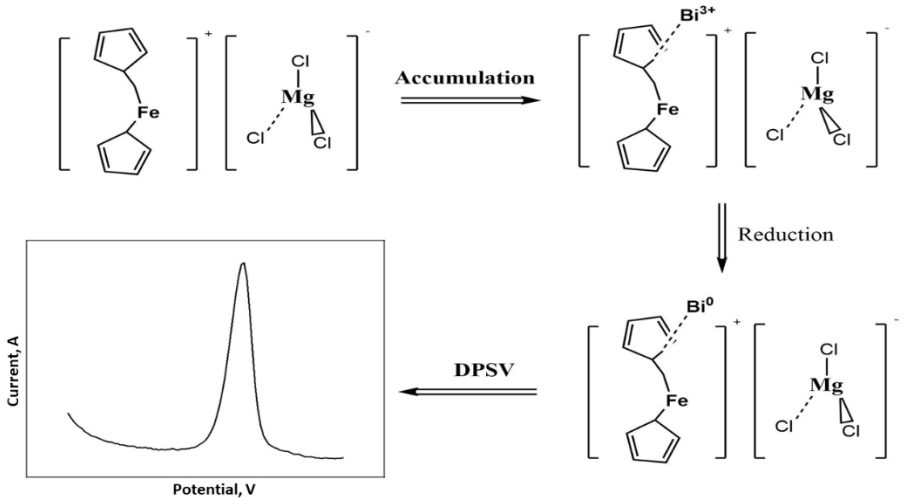

Figure 3. *Schematic illustration of the detection mechanism of Bi^{3+} at FTM modified electrode*

During the accumulation stage, Bi^{3+} ions interact with the FTM-modified electrode surface through coordination and electrostatic association, as depicted in the schematic representation of the complex structures. The FTM framework provides both anionic sites and a redox centre that facilitate the localization of Bi^{3+} at the electrode interface. This pre-concentration process is crucial because it markedly increases the surface density of the target ion prior to electrochemical conversion. As a result, the presence of FTM significantly enhances the electrode's ability to capture Bi^{3+}, directly influencing the magnitude of the analytical response obtained in the stripping step.

Upon applying a reducing potential, the accumulated Bi^{3+} ions undergo electrochemical transformation to metallic Bi, as reflected by the change in oxidation state in the schematic. At this stage, FTM not only contributes to initial ion capture but also maintains an electrochemically favourable environment for efficient electron transfer. This reduction produces a thin deposit of Bi on the electrode surface, serving as the active reservoir of analyte. The quantity of Bi formed is strongly correlated with the extent of the prior accumulation process, thereby determining the intensity of the anodic signal observed during stripping voltammetry.

In the final DPSV stage, the deposited Bi is reoxidized to Bi^{3+}, generating a well-defined anodic peak in the voltammogram, as illustrated in the schematic. The peak height is directly proportional to the amount of Bi present on the surface, and thus to the initial concentration of Bi^{3+} in the sample. The efficient accumulation and deposition enabled by the FTM modifier led to sharper and more intense stripping signals, ultimately improving the detection limit and analytical sensitivity. This mechanistic sequence demonstrates that FTM acts as an effective surface modifier, strengthening the electrochemical response to Bi^{3+} ions.

Variable experimental optimization

The effects of various experimental parameters on the stripping performance of Bi3+ at the FTM-modified electrode are shown in Figure 4. Optimizing these parameters is essential, since the electrochemical response strongly depends on the supporting electrolyte composition, ionic strength, and solution acidity, all of which control both the preconcentration of Bi^{3+} at the electrode surface and its subsequent electrochemical reduction. Different electrolytes (Na_2SO_4, KCl, KNO_3, NaCl and $NaNO_3$ at 0.05 M) were compared (Figure 4a). Among them, KCl produced the most pronounced and sharp stripping peak (I_p = 2.6 µA), while $NaNO_3$ gave the weakest response (I_p = 1.1 µA). This observation can be rationalized by considering the coordination chemistry of Bi^{3+}. Chloride ions exhibit a strong affinity toward Bi^{3+}, promoting the in-situ formation of Bi-Cl complexes (*e.g.* $BiCl_4^-$ or $BiCl_5^{2-}$), which are highly soluble and electrochemically active [32]. Such complexes enhance the accumulation efficiency at the electrode surface, leading to larger peak currents. In contrast, nitrate and sulphate ions do not coordinate effectively with Bi^{3+}, thereby limiting preconcentration and reducing sensitivity [33,34]. This finding is consistent with earlier reports that the presence of chloride is beneficial for stripping voltammetric analysis of Bi^{3+}.

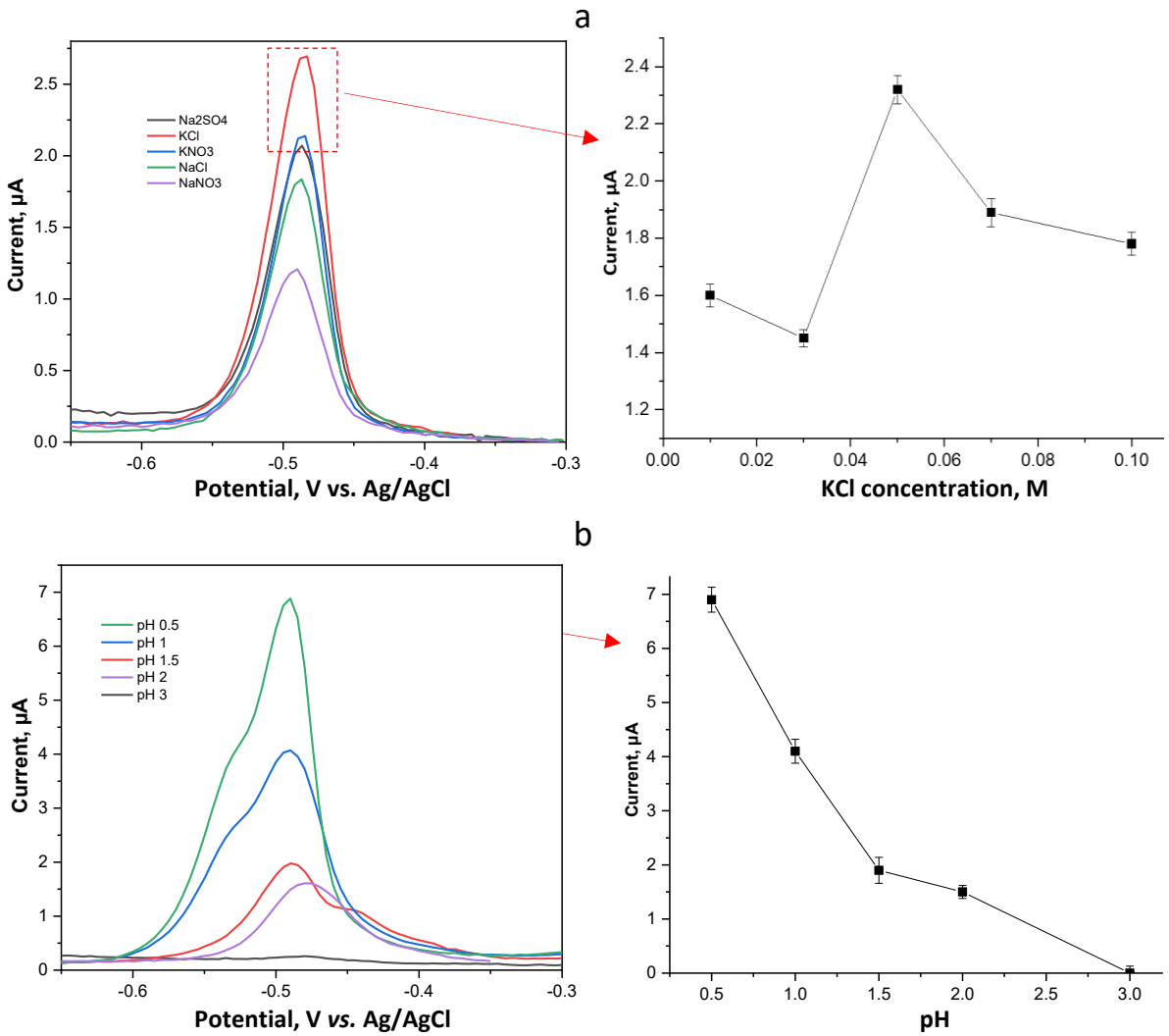

Figure 4. *(a) Differential pulse stripping voltammograms (DPSVs) of 1 mM Bi^{3+} at FTM modified electrode in various supporting electrolytes (0.05 M). The corresponding plot on the right shows the effect of different KCl concentrations (0.01-0.1 M) on the peak current; (b) DPSVs of 1.0 mM Bi^{3+} at different solution pH values (0.5 to 3.0). The corresponding plot on the right presents the variation of peak current as a function of pH. Experimental conditions: accumulation potential, -0.65 to -0.3 V; oxidation potential, -0.47 V*

The influence of KCl concentration was further investigated in the range of 0.01-0.1 M, as shown in the corresponding plot of Figure 4a. The stripping current increased steadily as the KCl concentration rose from 0.01 to 0.05 M, reaching a maximum at 0.05 M, followed by a gradual decrease at higher concentrations. This behaviour can be explained by two competing effects: (i) increasing chloride concentration enhances the formation of Bi-Cl complexes and reduces migration resistance [35], thereby favouring accumulation; (ii) at excessively high concentrations, the strong ionic strength alters the double-layer structure [36], reduces the diffusion rate of Bi^{3+} species, and may even induce competition between free chloride and FTM coordination sites. The net result is a decline in current response beyond the optimal concentration. Thus, 0.05 M KCl provides the best compromise between complex stabilization and efficient mass transport.

Solution acidity was found to play a decisive role in Bi^{3+} detection (Figure 4b). At strongly acidic pH of 0.5, the stripping peak current was highest (I_p = 6.9 µA), while progressive increases in pH led to a sharp decline in response, with the current nearly disappearing at pH 3.0. The explanation lies in the hydrolysis chemistry of Bi^{3+}: at higher pH values, Bi^{3+} undergoes hydrolysis to form insoluble species such as $Bi(OH)_3$, which precipitate and are unavailable for electrochemical deposition [37]. In contrast, under acidic conditions, Bi^{3+} remains fully soluble and stable, enabling efficient deposition onto the electrode surface and subsequent oxidative stripping. This trend corroborates well-established knowledge that stripping analysis of bismuth is best conducted in strongly acidic chloride media.

The optimization of DPSV parameters is crucial for achieving maximum sensitivity, reproducibility, and resolution in the detection of Bi^{3+} using a working electrode modified with FTM. The parameter study presented in Figure 5 demonstrates how pulse amplitude, step size, pulse increment, pulse time, accumulation time, and equilibration time influence the stripping signal of Bi^{3+}. The effect of pulse amplitude on the peak current response was investigated by varying the pulse amplitude from 5 to 25 mV, as shown in Figure 5a. An increase in pulse led to a progressive enhancement of the peak current, indicating improved perturbation of the electrochemical system and enhanced faradaic response. The highest peak current was obtained at a pulse of 25 mV, beyond which no further improvement was observed. Therefore, a pulse amplitude of 25 mV was selected as the optimum value for subsequent measurements.

Figure 5b illustrates the influence of step size on the peak current. The current response initially increased with increasing step size and reached its maximum at 5 mV, suggesting effective potential modulation and adequate signal resolution. At lower step sizes, the peak current was reduced, while excessive step sizes may compromise signal stability. Consequently, a step size of 5 mV was chosen as the optimum condition. The effect of pulse increment on the electrochemical response is presented in Figure 5c. The peak current increased steadily as the pulse increment was raised from 0.5 to 2.5 mV, indicating enhanced electron transfer kinetics and stronger analytical signals. Further increases did not yield significant improvement, suggesting a saturation effect. Thus, a pulse increment of 2.5 mV was selected as the optimal value.

Figure 5d shows the dependence of peak current on pulse time. An inverse relationship was observed, where increasing pulse time resulted in a gradual decrease in peak current. Longer pulse durations may promote diffusion-layer expansion and capacitive charging, which suppresses the faradaic response. The shortest pulse time of 0.1 s provided the highest peak current and was therefore selected as the optimal pulse time. The influence of accumulation time on the peak current is depicted in Figure 5e. The peak current increased with prolonged accumulation time, reaching a maximum at 150 s, likely due to enhanced analyte preconcentration at the electrode surface. Beyond this duration, the improvement became marginal, indicating surface saturation. Hence, an

accumulation time of 150 s was selected as the optimum condition. Figure 5f presents the effect of equilibration time on the electrochemical response. A gradual increase in peak current was observed with increasing equilibration time, reflecting improved stabilization of the electrochemical system prior to measurement. The maximum peak current was achieved at an equilibration time of 25 s, which was therefore adopted as the optimal equilibration time for all subsequent analyses.

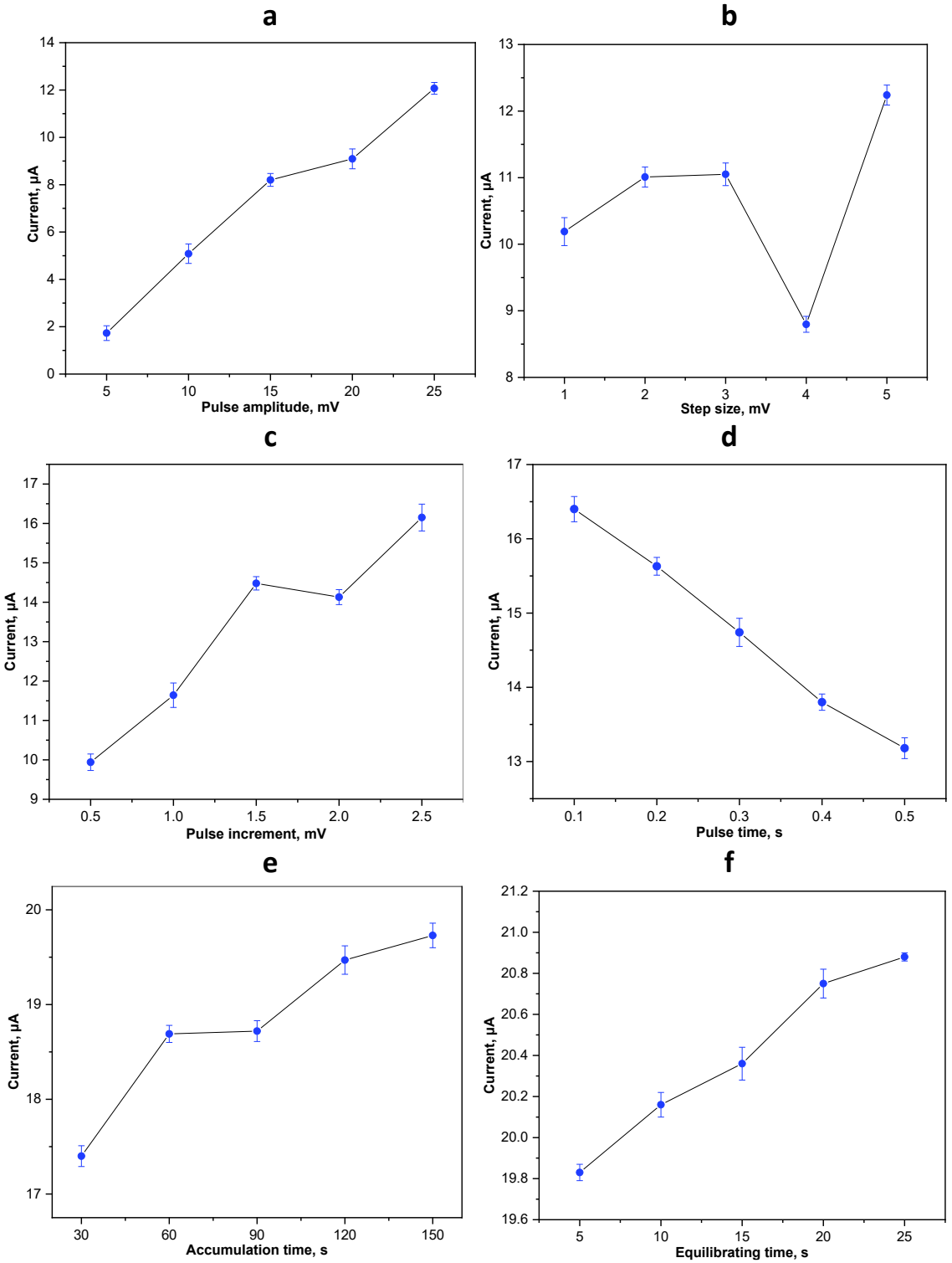

Figure 5. *DPSV parameters optimization for Bi^{3+} detection at FTM modified electrode: (a) pulse amplitude; (b) step size; (c) pulse increment; (d) pulse time; (e) accumulation time; and (f) equilibrating time. (Accumulation potential: -0.65 to -0.3 V; peak potential: -0.47 V; 0.05 M KCl; pH 0.5)*

Overall, the optimized DPSV parameters for Bi^{3+} detection using the FTM-modified electrode are pulse amplitude 25 mV, step size 5 mV, pulse increment 2.5 mV, pulse time 0.1 s, accumulation time 150 s, and equilibration time 25 s, under supporting electrolyte conditions of 0.05 M KCl at pH 0.5. The stripping peak of Bi^{3+} is observed at approximately -0.47 V, which aligns with the known redox behaviour of Bi^{3+} and is stabilized by the electron-donating properties of ferrocene and the coordination role of magnesium in the FTM. These results highlight that the modifier not only enhances sensitivity but also provides selective recognition of Bi^{3+} through synergistic electrochemical interactions. Further studies, including interference assessment with competing metal ions, stability of the FTM layer, and validation in real environmental water samples, are necessary to confirm the robustness and practical applicability of the developed sensor.

Calibration and detection limits

Under optimized electrochemical conditions, the calibration of Bi^{3+} was evaluated by differential pulse stripping voltammetry, yielding two linear ranges: 1.0 nM to 0.1 µM and 1.0 µM to 0.1 mM, as shown in Figure 6. The voltammogram clearly shows that the stripping peak current increases proportionally with the concentration of Bi^{3+}, with well-defined peaks centred around -0.47 V *vs.* Ag/AgCl, which is the characteristic redox potential of Bi^{3+}. At low concentrations, the current response is relatively small but remains distinguishable from the baseline, while at higher concentrations, a sharp and intense peak is observed, reflecting the efficient pre-concentration of Bi^{3+} ions onto the FTM-modified electrode surface. The calibration plots, divided into two linear ranges, are shown on the right side of the figure. The high concentration range yields a regression equation of I_p = 17.896 + 2.078 log $C_{Bi^{3+}}$ with R^2 = 0.996, whereas the low concentration range follows the equation I_p= 0.906 + 0.8546 log $C_{Bi^{3+}}$ with R^2= 0.982. These results confirm the strong linearity between peak current and Bi^{3+} concentration in both ranges, thereby validating the quantitative applicability of the developed method.

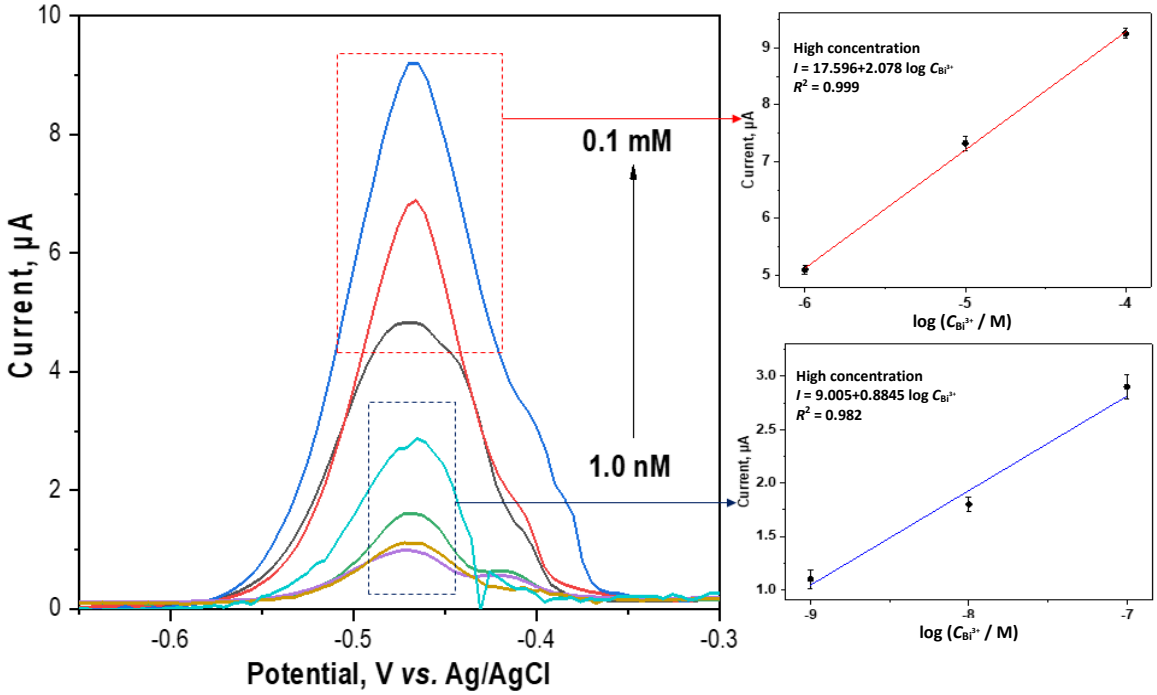

Figure 6. *DPSVs for the calibration plots at low and high concentrations of Bi^{3+} (right) at FTM modified electrode, recorded under optimum conditions (accumulation potential: -0.65 to -0.3 V; peak potential: -0.47 V; 0.05 M KCl; pH 0.5; pulse amplitude 25 mV; step potential 5 mV; pulse increment 2.5 mV; pulse duration 0.1 s; accumulation time 150 s; equilibration time 25 s)*

Importantly, the method exhibits an outstanding limit of detection (LoD) of 0.543 nM, calculated based on the signal-to-noise ratio criterion (S/N = 3) using Equation (3), where σ is the standard deviation of the blank signal, and s is the slope of the calibration curve.

$$LoD = 3\sigma / s \quad (3)$$

This ultra-low detection limit highlights the superior sensitivity of the FTM-modified electrode, enabling trace analysis of Bi^{3+} in aqueous environments where its concentration is typically very low. Such performance can be attributed to the synergistic effect of ferrocene, which facilitates fast electron transfer, and magnesium, which stabilizes the Bi^{3+} complex during the accumulation step, thereby improving the stripping efficiency. The reproducible and sharp stripping peaks further demonstrate the reliability of the electrode surface, while the wide dynamic range from nanomolar to millimolar concentrations confirms the robustness of the developed sensor. Collectively, these findings demonstrate that the FTM-modified electrode is highly effective for sensitive, selective, and quantitative detection of Bi^{3+}, with potential applications in monitoring trace bismuth contamination in environmental and industrial water samples.

To benchmark the performance of the proposed FTM-modified electrode, Table 1 compares its analytical figures of merit with previously reported methods for Bi^{3+} detection. The results show that this work achieves a lower detection limit and a wider linear range than most reported approaches, underscoring the effectiveness of the FTM integrated with carbon nanostructures.

Table 1. *Comparative study with previous research on Bi^{3+} detection using different techniques*

Recognition element	Technique	Linearity	LoD	Ref.
2-(benzothiazolylazo)-1,6-naphthalenediol (BTAND)	UV-VIS absorbance	35.9 nM to 1.05 µM	10.8 nM	[38]
GMP-Eu-DPA coordination polymer	Luminescence spectroscopy	1 µM to 230 µM	0.6 µM	[39]
Cerium zirconium phosphotungstate (CZPT)	Potentiometry	0.33 µM to 0.1 M	0.1 µM	[40]
Silkworm-derived carbon nanorods (swCNR)	Fluorescence spectroscopy	175 nM	0.5 to 5 µM	[41]
PPM-1 fibre (immobilized support)	Spectrophotometry (reflectance & absorbance)	0.57 µM to 8 µM	0.48 µM	[42]
Aliquat® 336 loaded poly(vinylidene-fluoride-co-hexafluoropropylene)	Solid-phase extraction (SPE)	0.019 µM to 9.6 µM	0.0057 µM	[43]
Nitrogen-doped carbon quantum dots (N-CQDs)	Fluorescence	0.95 to 61.5 µM	0.365 µM	[44]
(E)-4-methyl-N'-((2,3,6,7-tetrahydro-1H,5H-pyrido[3,2,1-ij]quinolin-9-yl)methylene)benzenesulfonohydrazide (L)	Fluorescence spectroscopy	0.1 µM to 10 µM and 0.01 µM to 1 µM	170 nM & 6.39 nM	[45]
Ferrocenium tetrachloromagnesate (FTM)	Different pulse stripping voltammetry	1.0 nM to 0.1 µM and 1.0 µM to 0.1 mM	0.543 nM	This work

Based on the literature review (Table 1), recent studies on the detection of Bi^{3+} ions have been predominantly focused on spectroscopic methods, with only a few reports employing solid-phase extraction (SPE) or potentiometric approaches. Carbon-based nanomaterials and Eu(III)-coordination polymers have been explored; however, the limitation of relatively high LoD, often up to the sub-micromolar range, remains a major challenge. Interestingly, no recent reports have been found utilizing voltammetric techniques for Bi^{3+} detection, despite their well-known advantages of higher sensitivity and selectivity. This study addresses this gap by introducing FTM as a recognition element in DPSV, achieving an exceptionally low LOD of 0.543 nM and two distinct linear ranges of 1.0 nM to 0.1 µM and 1.0 µM to 0.1 mM. This significant improvement underscores that the

integration of FTM with stripping voltammetry offers a promising approach for monitoring Bi^{3+}, while simultaneously opening new avenues for similar applications in the detection of other hazardous heavy metal ions in both environmental and biomedical domains.

Interference, reproducibility and repeatability

The interference study was carried out to evaluate the selectivity of the FTM-modified electrode toward Bi3+ detection in the presence of coexisting ions. As shown in Table 2, when interfering ions such as Mn^{2+}, La^{3+}, Ni^{2+}, Li^{+}, Zn^{2+}, Fe^{2+}, Cd^{2+}, Cu^{2+}, Er^{2+}, Ca^{2+}, and Pb^{2+} were introduced at concentrations ten times higher than Bi^{3+}, the percentage change in the DPSV experiments was relatively small, generally below 5 %. This finding indicates that at environmentally relevant levels, the tested ions do not significantly affect the stripping response of Bi^{3+}. Hence, the sensor demonstrates good tolerance against moderate levels of interfering species, confirming its high selectivity and suitability for practical applications in complex aqueous environments.

***Table 2**. Effect of concentration increase of interfering ions on detection of Bi^{3+} by DPSV*

Ion	Signal changes, %	
	100-fold	10-fold
Mn^{2+}	12.1 ± 0.4	3.2 ± 0.2
La^{3+}	14.7 ± 0.5	5.1 ± 0.3
Ni^{2+}	13.5 ± 0.5	4.3 ± 0.2
Li^{+}	11.6 ± 0.4	3.3 ± 0.3
Zn^{2+}	14.6 ± 0.3	6.2 ± 0.4
Fe^{2+}	13.2 ± 0.4	4.3 ± 0.3
Cd^{2+}	16.7 ± 0.4	7.4 ± 0.2
Cu^{2+}	14.9 ± 0.4	4.3 ± 0.3
Er^{3+}	12.3 ± 0.3	3.2 ± 0.3
Ca^{2+}	14.8 ± 0.4	2.2 ± 0.4
Pb^{2+}	15.2 ± 0.2	7.1 ± 0.3

At much higher concentrations, *i.e.* when interfering ions were present at 100-fold excess, some ions such as Pb^{2+} and Cd^{2+} caused more pronounced effects, with current changes reaching 15.2 and 16.7 % respectively. This suggests competitive interactions during the accumulation process, where these ions may compete with Bi^{3+} for adsorption or coordination sites on the electrode surface. Nevertheless, even under such extreme conditions, the Bi^{3+} signal remained clearly identifiable, demonstrating the robustness of the developed system. These results highlight that the FTM-modified electrode can maintain reliable performance under realistic conditions, with interference becoming significant only in cases of extraordinarily high ion concentrations that are rarely encountered in natural samples.

Reproducibility was evaluated using five independently fabricated electrodes, as shown in Figure 8a. The current responses were consistent, yielding a relative standard deviation (RSD) of 8.57 %. This relatively low variability demonstrates that the electrode fabrication process, including the modification with the FTM, is highly reliable and can be reproduced with good consistency. The small differences observed among electrodes indicate that the preparation protocol is robust, suggesting that the method can be scaled for batch production without compromising performance.

Repeatability was further assessed using a single electrode tested for ten consecutive measurements, as shown in Figure 8b. The results revealed stable current responses with an RSD of 7.77 %,

confirming that the electrode maintains its sensitivity and functionality after repeated use. This finding is particularly important for practical sensing applications, as it ensures that the electrode does not degrade or lose activity quickly during multiple cycles of operation. Overall, the reproducibility and repeatability studies strongly support the robustness and reliability of the FTM-modified electrode, complementing its high sensitivity, low detection limit, and good selectivity for Bi^{3+} detection in real-world environmental monitoring.

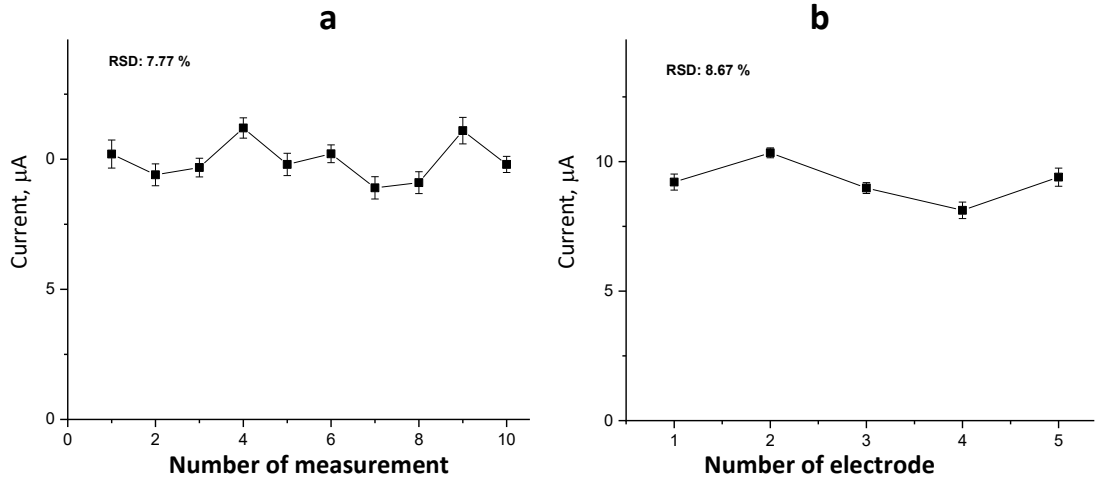

Figure 8. *(a) reproducibility and (b) repeatability set of 0.1 mM Bi^{3+} at FTM modified electrode(s) under optimum conditions (accumulation potential: -0.65 V to -0.3 V; peak potential: -0.47 V; 0.05 M KCl; pH 0.5; pulse amplitude of 25 mV; step potential of 5 mV; pulse increment of 2.5 mV; pulse duration of 0.1 s; accumulation period of 150 s; equilibration time of 25 s)*

Real samples

The applicability of the FTM-modified electrode was further evaluated by analysing real water samples collected from four river sites and tap water, as summarized in Table 3. Since no Bi^{3+} was detected in the original unspiked samples, the standard addition method was applied by spiking each sample with 1.0 mM of Bi^{3+}. The measured concentrations were then compared to the spiked values to calculate recovery and relative standard deviation (RSD). The recovery values ranged between 89 and 104 %, while the RSD values remained relatively low, between 2.4 % and 5.4 %. These results confirm that the developed sensor is capable of accurately detecting Bi^{3+} in complex environmental matrices without significant matrix effects that could compromise the analytical performance.

Table 3*. Real samples analysis of Bi^{3+} using FTM modified electrode*

Sample	Amount, mM		Recovery, %
	Spiked	Found	
River 1	1.0	0.89 ± 0.03	89
River 2	1.0	0.96 ± 0.04	96
River 3	1.0	0.92 ± 0.02	92
River 4	1.0	0.97 ± 0.04	97
Tap water	1.0	1.04 ± 0.06	104

The slight variations observed in recovery across different samples can be attributed to differences in the physicochemical properties of the water, such as ionic strength, dissolved organic matter, or other minor constituents that could interact with Bi^{3+} during the accumulation process. Notably, recoveries close to 100 % for most river samples (92 to 97 %) and tap water (104 %) demonstrate that the sensor can reliably quantify Bi^{3+} in both natural and treated water systems.

The acceptable RSD values further highlight the precision of the method, reinforcing its suitability for real-world monitoring applications. Collectively, these findings strongly validate the robustness, accuracy, and applicability of the FTM-modified electrode as a practical sensing platform for trace Bi^{3+} analysis in environmental waters.

Conclusions

In this work, a ferrocenium tetrachloromagnesate-modified multi-walled carbon nanotube (MWCNT) electrode was developed for the sensitive and selective detection of Bi^{3+} in aquatic systems. The synergistic role of magnesium within the redox-active FTM significantly enhanced electron transfer kinetics and electrochemical conductivity, as confirmed by structural and electrochemical characterizations. Optimization studies revealed that 10 wt.% FTM loading provided the best interfacial properties. The fabricated sensor demonstrated an ultralow detection limit of 0.543 nM and two broad linear ranges of 1.0 nM to 0.1 µM and 1.0 µM to 0.1 mM, excellent reproducibility and stability, as well as strong selectivity against potentially interfering ions. Furthermore, successful application to real water samples, with recoveries between 89 and 104 %, validates its practical utility for environmental monitoring. Overall, this study highlights the promise of magnesium-based complexes integrated with carbon nanostructures as advanced electrode modifiers for the trace-level detection of toxic metals, opening pathways for the development of efficient and reliable electrochemical sensors in environmental analysis.

Acknowledgements: *The authors would like to express their sincere gratitude to the Universiti Pendidikan Sultan Idris, Tanjong Malim, Perak, Malaysia for providing the respective financial support Geran Penyelidikan Universiti (GPU TOPDOWN : 2016-0220-102-41) and Universitas Negeri Padang, West Sumatera, Indonesia, for providing the necessary facilities and support that made this research possible.*

References

[1] H. Li, B. Cheng, J. Zhang, X. Zhou, C. Shi, L. Zeng, C. Wang, Recent advances in the application of bismuth-based catalysts for degrading environmental emerging organic contaminants through photocatalysis, *Journal of Environmental Chemical Engineering* **11** (2023) 110371. https://doi.org/10.1016/j.jece.2023.110371

[2] M. Zacchini, Bismuth interaction with plants: Uptake and transport, toxic effects, tolerance mechanisms, *Chemosphere* **360** (2024) 142414. https://doi.org/10.1016/j.chemosphere.2024.142414

[3] S. A. Shetu, L. M. Sanchez-Palestino, G. Rivera, D. Bandyopadhyay, Medicinal bismuth: Bismuth-organic frameworks as pharmaceutically privileged compounds, *Tetrahedron* **129** (2022) 133117. https://doi.org/10.1016/j.tet.2022.133117

[4] M. Fadhlaoui, N.J.T. Pearce, I. Lavoie, C. Fortin, Interactive effects of bismuth exposure (water and diet) and temperature on snail fatty acid composition, antioxidant enzymes and lipid peroxidation, *Frontiers in Environmental Chemistry* **5** (2024) 1332967. https://doi.org/10.3389/fenvc.2024.1332967

[5] F. Pietrini, L. Passatore, S. Carloni, L. Massimi, M. L. Astolfi, C. Giusto, M. Zacchini, Bismuth exposure affects morpho-physiological performances and the ionomic profile in garden cress (*Lepidium sativum* L.) plants, *Frontiers in Environmental Science* **11** (2023) 1221573. https://doi.org/10.3389/fenvs.2023.1221573

[6] S. Kolesnikov, T. Minnikova, K. Kazeev, Y. Akimenko, N. Evstegneeva, Assessment of the ecotoxicity of pollution by potentially toxic elements by biological indicators of Haplic

Chernozem of Southern Russia (Rostov region), *Water, Air, & Soil Pollution* **233** (2022) 18. https://doi.org/10.1007/s11270-021-05496-3

[7] S. Gavrilaș, F. L. Burescu, B. D. Chereji, F. D. Munteanu, The Impact of anthropogenic activities on the catchment's water quality parameters, *Water* **17** (2025) 1791. https://doi.org/10.3390/w17121791

[8] D. S. Chormey, E. Ö. Er, S. E. Bodur, B. T. Zaman, S. Bodur, T. B. Kustanto, İ. Kayın, S. Bakırdere, Trace element determination using mass spectrometry coupled detection methods, *Trends in Environmental Analytical Chemistry* **45** (2025) e00257. https://doi.org/10.1016/j.teac.2024.e00257

[9] R. Lindenmayer, L. Lu, F. Eivazi, Z. Afrasiabi, Atomic spectroscopy-based analysis of heavy metals in seaweed species, *Applied Sciences* **13** (2023) 4764. https://doi.org/10.3390/app13084764

[10] M. Madadelahi, F. O. Romero-Soto, R. Kumar, U. B. Tlaxcala, M. J. Madou, Electrochemical sensors: Types, applications, and the novel impacts of vibration and fluid flow for microfluidic integration, *Biosensors and Bioelectronics* **272** (2025) 117099. https://doi.org/10.1016/j.bios.2024.117099

[11] A. Shabib, M.A. Maraqa, A.F. Mohammad, F. Awwad, Design, fabrication, and application of electrochemical sensors for microplastic detection: a state-of-the-art review and future perspectives, *Environmental Sciences Europe* **37** (2025) 94. https://doi.org/10.1186/s12302-025-01138-1

[12] A. Nofriandi, I. Isa, N. Hashim, M. Idris, M. Syahrizal, I. Dewata, Ultrasensitive voltammetric sensor based on ferrocenium tetrachloroferrate for determination of manganese(II) in water pollutant, *Materials Chemistry and Physics* **339** (2025) 130725. https://doi.org/10.1016/j.matchemphys.2025.130725

[13] X. Zhou, Electrochemical detection of heavy metal ions in water using MWCNT/ZnO nanocomposite, *International Journal of Electrochemical Science* **19** (2024) 100559. https://doi.org/10.1016/j.ijoes.2024.100559

[14] P. J. Obeid, N. Sari-Chmayssem, P. Yammine, D. Homsi, H. El-Nakat, Z. Matar, S. Hamieh, D. Koumeir, A. Chmayssem, Designs and materials of electrodes for electrochemical sensors, *ChemElectroChem* **12** (2025) e202500230. https://doi.org/10.1002/celc.202500230

[15] R. Singh, R. Gupta, D. Bansal, R. Bhateria, M. Sharma, A Review on recent trends and future developments in electrochemical sensing, *ACS Omega* **9** (2023) 7336-7356. https://doi.org/10.1021/acsomega.3c08060

[16] M. Mulyawati, K. A. Madurani, I. Ulfin, N. P. Sari, F. Kurniawan, Development of a copper-modified iron electrode electrochemical sensor for sensitive detection of oxalic acid, *Materials Chemistry and Physics* **344** (2025) 131063. https://doi.org/10.1016/j.matchemphys.2025.131063

[17] J. Kim, J. Ling, Y. Lai, P.J. Milner, Redox-active organic materials: From energy storage to redox catalysis, *ACS Materials Au* **4** (2024) 258-273. https://doi.org/10.1021/acsmaterialsau.3c00096

[18] X. Du, Z. Lin, X. Wang, K. Zhang, H. Hu, S. Dai, Electrode materials, structural design, and storage mechanisms in hybrid supercapacitors, *Molecules* **28** (2023) 6432. https://doi.org/10.3390/molecules28176432

[19] D. V. Estrada-Osorio, R. A. Escalona-Villalpando, A. Gutiérrez, L. G. Arriaga, J. Ledesma-García, Poly-L-lysine-modified with ferrocene to obtain a redox polymer for mediated glucose biosensor application, *Bioelectrochemistry* **146** (2022) 108147. https://doi.org/10.1016/j.bioelechem.2022.108147

[20] S. Nuthana Kalva, F. Ali, M. Koç, Recent advances in the post-processing of magnesium based scaffolds for orthopedic applications, *Next Materials* **6** (2025) 100295. https://doi.org/10.1016/j.nxmate.2024.100295
[21] V. Tsakiris, C. Tardei, F. M. Clicinschi, Biodegradable Mg alloys for orthopedic implants - A review, *Journal of Magnesium and Alloys* **9** (2021) 1884-1905. https://doi.org/10.1016/j.jma.2021.06.024
[22] J. Xie, T. Zhang, J. Jiang, W. Xue, W. Wang, J. Ni, X. Zhang, X. Liu, Advances in magnesium-based implants for biomedical applications: A comprehensive review and future perspectives, *Journal of Magnesium and Alloys* **13** (2025) 2978-3003. https://doi.org/10.1016/j.jma.2025.05.009
[23] H. Strzelecka-Gołaszeska, A. Woźniak, T. Hult, U. Lindberg, Effects of the type of divalent cation, Ca^{2+} or Mg^{2+}, bound at the high-affinity site and of the ionic composition of the solution on the structure of F-actin, *Biochemical Journal* **316** (1996) 713-721. https://doi.org/10.1042/bj3160713
[24] Y. Luo, L. Liu, H. Wang, T. Liu, H. Li, B. Tan, Y. Pan, A. Liu, J. Cheng, Research progress on the corrosion behavior of magnesium alloys in natural environments, *Materials Today Communications* **48** (2025) 113433. https://doi.org/10.1016/j.mtcomm.2025.113433
[25] Y. Kang, K. Zhang, X. Lin, Surface modifications of magnesium-based materials for hydrogen storage and nickel-metal hydride batteries, *Coatings* **13** (2023) 1100. https://doi.org/10.3390/coatings13061100
[26] T. Zhang, W. Wang, J. Liu, L. Wang, Y. Tang, K. Wang, A review on magnesium alloys for biomedical applications, *Frontiers in Bioengineering and Biotechnology* **10** (2022) 953344. https://doi.org/10.3389/fbioe.2022.953344
[27] R. Kumar, S. Kumar, A.J. Kailath, R.K. Sahu, Mechanistic investigation of hydrogen generation from water and magnesium catalyst reaction: Advanced reactive molecular dynamics simulation, *International Journal Hydrogen Energy* **52** (2024) 1440-1445. https://doi.org/10.1016/j.ijhydene.2023.07.247
[28] K. K. Thomas, M. N. Zafar, W. G. Pitt, G.A. Husseini, Biodegradable magnesium alloys for biomedical implants: Properties, challenges, and surface modifications with a focus on orthopedic fixation repair, *Applied Sciences* **14** (2024) 10. https://doi.org/10.3390/app14010010
[29] S. Mehanathan, J. Jaafar, A. M. Nasir, A. F. Ismail, T. Matsuura, M. H. D. Othman, M. A. Rahman, N. Yusof, Magnesium oxide nanoparticles for the adsorption of pentavalent arsenic from water: Effects of calcination, *Membranes* **13** (2023) 475. https://doi.org/10.3390/membranes13050475
[30] B. Liu, H. Guo, L. Sun, Z. Pan, L. Peng, M. Wang, N. Wu, Y. Chen, X. Wei, W. Yang, Electrochemical sensor based on covalent organic frameworks/MWCNT for simultaneous detection of catechol and hydroquinone, *Colloids and Surfaces A* **639** (2022) 128335. https://doi.org/10.1016/j.colsurfa.2022.128335
[31] Y. Yulkifli, W. P. Yandes, I. M. Isa, N. Hashim, A. Ulianas, S. N. M. Sharif, M. I. Saidin, M. S. Ahmad, S. N. A. M. Yazid, S. Suyanta, R. Nuryadi, N. Abd Azis, A nanocomposite paste electrode sensor for simultaneous detection of uric acid and bisphenol A using zinc hydroxide nitrate-sodium dodecylsulfate Bispyribac, *Sensors* **23** (2023) 8366. https://doi.org/10.3390/s23208366
[32] L. Johansson, K. Haugsten, H. H. Bruun, O. Smidsrød, A. A. Lindberg, G. Jansen, B. Lamm, B. Samuelsson, The complex formation of bismuth(III) with chloride in aqueous solution. A solubility study., *Acta Chemica Scandinavica* **23** (1969) 548-556. https://doi.org/10.3891/acta.chem.scand.23-0548
[33] V. Baibakova, K. Cruse, M. G. Taylor, C. M. Sutter-Fella, G. Ceder, A. Jain, S. M. Blau, Precursor reaction pathway leading to BiFeO3 formation: insights from text-mining and

chemical reaction network analyses, *Digital Discovery* **4** (2025) 1602-1611. https://doi.org/10.1039/d5dd00160a

[34] H. Bhatia, J. Guo, C. N. Savory, M. Rush, D. I. James, A. Dey, C. Chen, D. K. Bučar, T. M. Clarke, D. O. Scanlon, R. G. Palgrave, B. C. Schroeder, Exploring bismuth coordination complexes as visible-light absorbers: Synthesis, characterization, and photophysical properties, *Inorganic Chemistry* **63** (2024) 416-430. https://doi.org/10.1021/acs.inorgchem.3c03290

[35] X. S. Wang, A. E. Williams-Jones, R. Z. Hu, Q. Liu, F. X. Liu, Y. Mei, Z. Q. Jiang, L. B. Shang, J.J. Zhu, X. W. Bi, The transport of bismuth in HCl-bearing aqueous vapour and low-density aqueous supercritical fluids: Implications for natural systems, *Geochimica et Cosmochimica Acta* **378** (2024) 203-216. https://doi.org/10.1016/j.gca.2024.06.008

[36] K. Yamashita, K. Komatsu, H. Kagi, Crystal structure of potassium chloride monohydrate: water intercalation into the B1 structure of KCl under high pressure, *Acta Crystallographica Section C* **78** (2022) 749-754. https://doi.org/10.1107/S2053229622011135

[37] D. B. Kleja, J. P. Gustafsson, V. Kessler, I. Persson, Bismuth(III) forms exceptionally strong complexes with natural organic matter, *Environmental Science & Technology* **56** (2022) 3076-3084. https://doi.org/10.1021/acs.est.1c06982

[38] A. H. Alanazi, A. S. Al-zbedy, R. El-sayed, K. F. Debbabi, A. S. Amin, A. S. Al-zbedy, Eco-friendly optical sensor for detecting bismuth(III) ions in environmental , pharmaceutical , and biological sources, *Chinese Journal of Analytical Chemistry* **53** (2025) 100591. https://doi.org/https://doi.org/10.1016/j.cjac.2025.100591

[39] Y. Jiang, D. Tai, Z. Xiao, J. Liu, Ratiometric luminescence detection of Bi3+ ions in water using a europium coordination polymer, *Spectroscopy Letters* **58** (2025) 445-452. https://doi.org/10.1080/00387010.2024.2447519

[40] R.F. Aglan, M.M. Hamed, H.M. Saleh, A new screen-printed electrode for selective determination of bismuth in different authentic samples, *Journal of the Iranian Chemical Society* **20** (2023) 1481-1490. https://doi.org/10.1007/s13738-023-02771-4

[41] N. Sharma, A. Sharma, M. Park, H.J. Lee, Silkworm-derived carbon nano rods (swCNR) for detection of bismuth ions (Bi^{3+}) in aquatic medium and their antiradical properties, *Heliyon* **10** (2024) e33572. https://doi.org/10.1016/j.heliyon.2024.e33572

[42] Z. Smanova, B. Normatov, U. Ahmadjonov, S. Rakhimov, B. Shodmonov, E. Berdimurodov, W. M. N. B Wan Nik, I. Eliboev, G. K. Ziyayeva, O. Baigenzhenov, A. Hosseini-Bandegharaei, Sorption-spectrophotometric determination of bismuth ion (III) using immobilised xylenol orange on modified polyacrylonitrile, *International Journal of Environmental Analytical Chemistry* **105** (2025) 5859–5879. https://doi.org/10.1080/03067319.2024.2405067

[43] J. A. Rajabi-Orhani, L. Dolatyari, M. Reza Yaftian, A different application of the Aliquat® 336 loaded poly(vinylidene fluoride-co-hexafluoropropylene) based electrospun nanofibers disks for the preconcentration followed by flame atomic absorption spectrometry detection of low-level Bi3+, *Microchemical Journal* **207** (2024) 111703. https://doi.org/10.1016/j.microc.2024.111703

[44] Anoushka, M. Rani, U. Shanker, Rapid microwave assisted synthesis of N-doped CQDs for highly selective 'turn-off' sensing of bismuth(III) ions in wastewater, *Analytica Chimica Acta* **1351** (2025) 343904. https://doi.org/10.1016/j.aca.2025.343904

[45] L. K. Shaji, J. Jose, R. Bhaskar, R. Selva Kumar, V. Vetriarasu, S. G. Bhat, S. K. Ashok Kumar, Smartphone assisted fluorescent-colorimetric probe for bismuth(III) ion and potential applications, *Inorganic Chemistry Communications* **147** (2023) 110252. https://doi.org/10.1016/j.inoche.2022.110252